Passive UWB Multiplexing device for a Single-Port MIMO RADAR

Thomas Fromenteze, Cyril Decroze and David Carsenat
(Affiliation): XLIM, University of Limoges, 123 av. Albert Thomas, 87000 Limoges, France, thomas.fromenteze@xlim.fr

***Abstract*—MIMO radar imaging is receiving a substantial attention, thanks to its high resolution capacity. Whereas, the complexity and the cost of the active devices able to simultaneously transmit and receive signals of each antenna is a disincentive for the expansion of this technology, particularly using UWB signals. In this paper, a passive device is presented to achieve MIMO radar imaging using a single-port reflection measurement.**

***Index Terms*—Beamforming, MIMO, UWB, Antenna array, Passive technique**

I. Introduction

The conventional radar systems use an antenna array to achieve beamforming: the waves reflected on the scene to image are received by a single antenna for different beam steering and a time-angle image can be computed. Conversely, a single antenna can light the scene and the reflected waveforms gathered by the antenna array can be delayed and summed to achieve beamforming. Recently, a new technique using antenna arrays for the transmission and the reception has received a substantial attention [1][2]. Indeed, the use of a multiple-input multiple-output (MIMO) system for radar imaging allows an improvement of the image resolution compared to conventional beamforming techniques [3]. The spatial diversity of the medium is exploited through the low level of transfer function's correlation between each antenna. Thus, independent signals can be sent to each receiving element by all the transmitters. MIMO radar can be applied to a wide range of applications such as medical diagnosis [4], through-wall imaging [5] and concealed weapon detection [6]. Whereas, a complex architecture is required to reach this resolution, presenting as much transmitting and receiving systems as ports involved in the MIMO radar.

In this paper, a single-port MIMO radar is introduced : by mean of a passive $1 \times N$ device able to perform a compression in the physical layer of the waveforms received by an antenna array, MIMO radar imaging is performed with a single-port reflection measurement.

II. Theoretical principle

The system presented in this paper is a mono-static MIMO radar, meaning that the same antenna array is used for both transmission and reception. A $1 \times N$ passive device is connected to the N antennas of the array. The purpose of this system is to achieve a physical compression of the received waveforms to get an unique coded signal containing all the information (Fig.1).

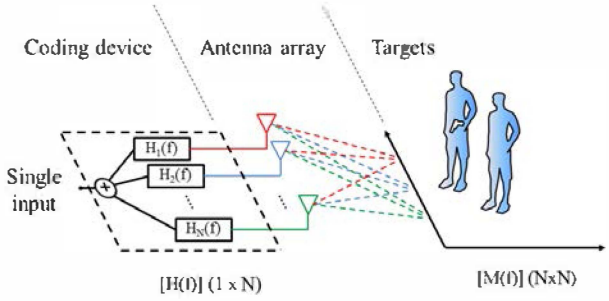

Fig. 1. Schematic principle of the single-port MIMO radar : A $1 \times N$ coding device is connected to an antenna array. The reflection measurement at its input port allows a compression of the scattering matrix $[M(f)]$ including the scene information, through the passive device transfer functions $[H(f)]$.

By measuring the reflected wave at the coding device's input port, the scattering matrix of a set of targets is compressed, leading to a measured signal $S(f)$:

$$S(f) = \underbrace{[H(f)]}_{1\times N}\underbrace{[M(f)]}_{N\times N}\underbrace{[H(f)]^T}_{N\times 1} \tag{1}$$

The wave emitted at the passive device's input is coded by the propagation in each channel $[H(f)]$ and distributed to the antenna array. The radiated waves are reflected on the targets to image and received by the antenna array. Thus, the frequency signals are multiplied by the scattering matrix $[M(f)]$, corresponding to the targets signature between each couple of transmitter-receiver. Then these waveforms are coded again by the propagation in the passive device and compressed in an unique signal $[S(f)]$ measured by a vector network analyzer. The scattering matrix is coded by the propagation in the passive device, so the useful data are compressed by transfer functions that has been pre-measured. Computing the pseudo-inverse of $[H(f)]$, the scattering matrix can be retrieved :

$$[M_r(f)] = [H(f)]^{-1}[S(f)]([H(f)]^{-1})^T \tag{2}$$

where $[M_r(f)]$ is the reconstructed matrix and $[H(f)]^{-1}$ is the pseudo inverse of the vector $[H(f)]$ calculated using a Tikhonov Regularization :

$$[H(f)]^{-1} = ([H(f)]^{\dagger}[H(f)] + \beta[I_N])[H(f)]^{\dagger} \tag{3}$$

with † the transpose-conjugate operator and $[I_N]$ the $N \times N$ identity matrix. The value of the scalar β prevents any ill-conditioning problem by adding a threshold to the inverted part. The aim of the transfer function pseudo-inverse is to cancel the compression applied to the signals by the propagation in the passive device. Thus, an ideal pseudo-inverse would satisfy the following condition :

$$[H(f)]^{-1}[H(f)] = [H(f)][H(f)]^{-1} = [I_N] \tag{4}$$

Developing the equation (2) with these ideal conditions, the reconstructed matrix $[M_r(f)]$ becomes :

$$[M_r(f)] = \underbrace{[H(f)]^{-1}[H(f)]}_{[I_N]}\,[M(f)]\,\underbrace{[H(f)]^T([H(f)]^{-1})^T}_{[I_N]} \tag{5}$$

$$[M_r(f)] = [M(f)] \tag{6}$$

leading to a perfect reconstruction of the scattering matrix $[M(f)]$.

In practice, the matrix reconstruction can not be perfect at a single frequency, but is improved in the time domain using the constructive effect of the egalization.

Furthermore, to get a good decoding the passive device's channels must have a low level of cross-correlation to avoid the projection of a signal on the others during the coding/decoding process. In a device with large delay spread channels impulse responses, the use of UWB signals allows the exploitation of the medium richness to decrease the cross-correlation level of channels [7]. If the conditions previously cited are satisfied, the MIMO radar imaging can be achieved using the setup depicted in the figure (1). Thus, images can be computed using a conventional delay-and-sum algorithm.

A reverberating cell of $1.1m \times 0.7m \times 0.6m$ is used to reach these particular conditions. The very large modal diversity in this over-sized cavity is well suited to get uncorrelated channels. Thus, UWB probes are randomly set in the cell and connected to each output (Fig. 2), leading to highly frequency selective channels between the input and the outputs. A metal plate is set in front of the input probe to avoid a common direct path to the output probes that could increase the correlation level between each channel impulse response.

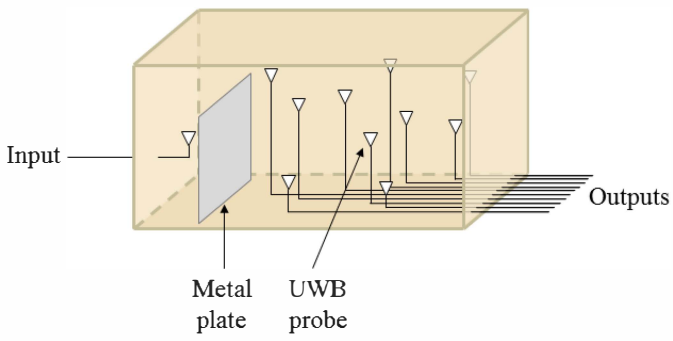

Fig. 2. Schematic of the reverberating cell used as a 1×10 passive device.

The reverberating cell's channels are measured in the 2-10 GHz band with a vector network analyzer *ZVL Rohde and Schwarz*, using 4001 frequency samples (Fig. 3). For each transmission measurement, all the remaining ports are connected to 50Ω SMA terminations.

Fig. 3. Picture of the reverberating cell used for this experiment, connected to a vector network analyzer (left). 21 UWB probes are randomly set in the cell to get a 1×20 passive device (right).

The matrix corresponding to the compression and decompression of the information can be analyzed to check if the channel are uncorrelated enough to retrieve the information. Using *Matlab*, the following inverse Fourier transform can be computed :

$$[R(t)] = \mathscr{F}^{-1}\left([H(f)]^{-1}[H(f)]\right) \tag{7}$$

For the sake of simplicity, the matrix $[R(t)]$ is referred as the correlation matrix of the device's channels. That name would be rigorously true only if β was large enough to get a pseudo-inverse equivalent to a phase-compensation, or time reversal in time domain. According to equation (4), the diagonal vectors of this matrix should ideally be dirac impulses, with all the other vectors remaining zero to ensure a proper reconstruction of the signals. The figure (4) depicts the autocorrelation $[R_{11}(t)]$ of the first channel, compared to the intercorrelation $[R_{12}(t)]$ between the first and the second channel.

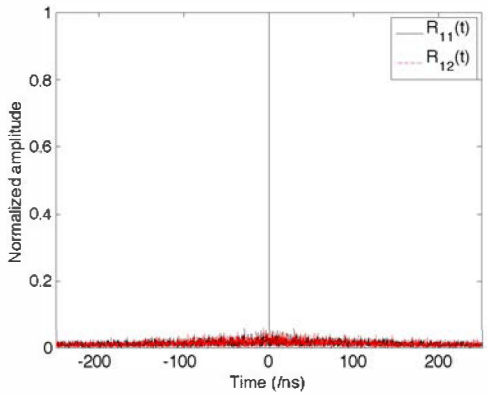

Fig. 4. Absolute value of the first channel's autocorrelation compared to the intercorrelation between the first and the second channel. The amplitudes are normalized by the autocorrelation maximum level.

The maximum value of each correlation's absolute value is depicted in the figure (5). An average ratio of 17 between the autocorrelations and the intercorrelations levels ensures a good reconstruction of the scattering matrix, with a low inter-signals projection.

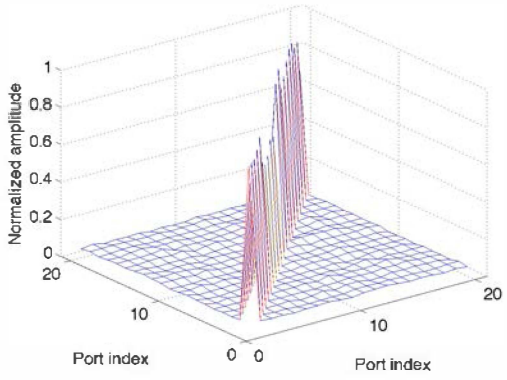

Fig. 5. Maximum values of the correlation between each couple of channels. The amplitudes are normalized by the highest autocorrelation level.

A simulation of near-field imaging is computed using the measured reverberating cell's channel to demonstrate the single-port MIMO imaging capacity of this device. A *Matlab* program simulates a 5×4 array made of isotropic antennas connected to the 20 channels of the cell. The inter-element space is set to $d = 2.5\ c\frac{2}{fmax+fmin} = 6.25cm$, with c the celerity of light. A $36cm \times 24cm$ weapon is positioned at a distance of $0.5m$ of the array (Fig. 6).

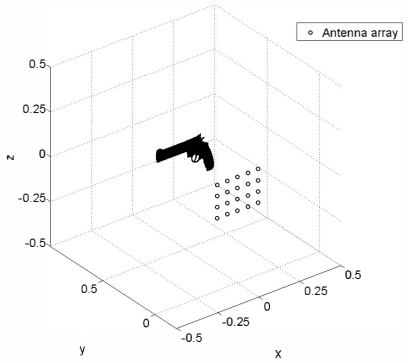

Fig. 6. Numerical simulation setup of the MIMO array in front of a weapon to image.

The scene is confined in a $1m \times 1m \times 1m$ volume, divided in $71 \times 71 \times 71$ voxels. Delays are applied to the scattering matrix elements to focus on each voxel (Fig. 7).

A front view is extracted from the 3D data at the weapon's distance (Fig. 8). The single-port imaging is less precise than the conventional MIMO method, but still presents the resolution required to detect the weapon.

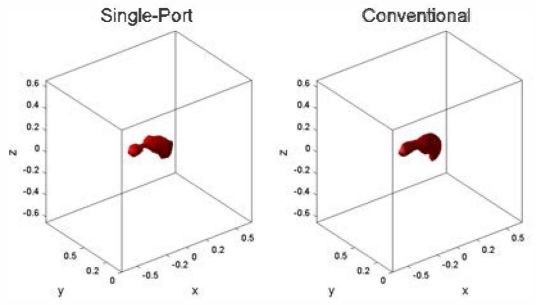

Fig. 7. 3D imaging of weapon using the a conventional MIMO system compared to the single-port MIMO device.

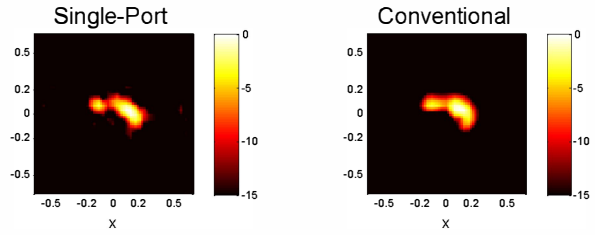

Fig. 8. Front view of the weapon for both conventional and single-port MIMO imaging.

III. Measurements

The reverberating cell has been connected to an 5×4 antenna array to measure radar images (Fig. 9). The antennas has been developed using the software *CST Microwave Studio* starting from [8], and optimized for a FR4-epoxy substrate in the $2 - 10\ GHz$ bandwidth. At first, a reflexion measurement is achieved at the passive device's input using the network analyzer without target in front of the antenna array.

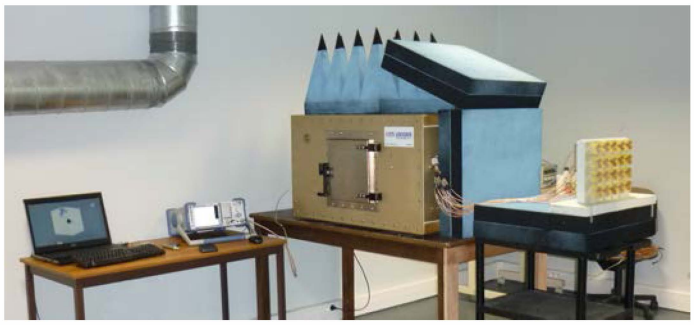

Fig. 9. Single-port MIMO imaging setup

Thus, the inter-element coupling is measured to be subtracted from the next measurements. Then, a target is set in front of the antenna array on a foam structure whom relative permittivity is close to 1. The target is a steel petanque ball of diameter $7.5\ cm$, set at a range of $50\ cm$ from the array (Fig. 10). The computed images are depicted in figure (11). The ball's position is correctly retrieved using this new technique of MIMO imaging.

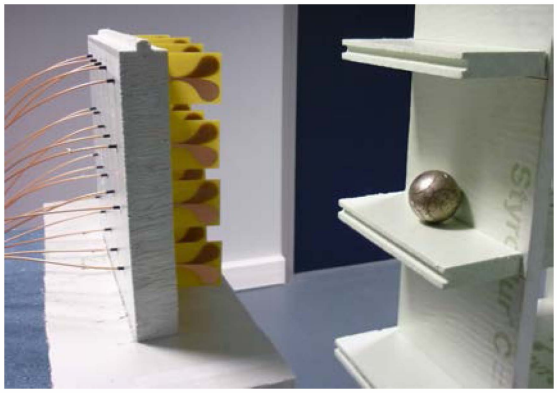

Fig. 10. Target position in front of the antenna array

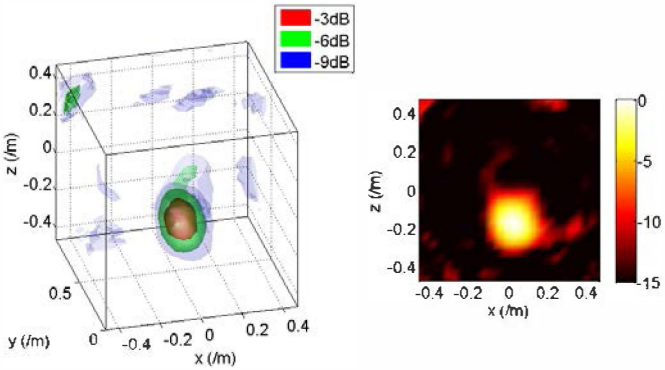

Fig. 11. Radar images measured using the petanque ball as target, in three dimensions (left) and in two dimensions at a range of 50 cm (right).

IV. Conclusion

A passive multiplexing device has been presented to achieve single-port MIMO imaging. The image resolution should be enhanced by increasing the number of antennas and by applying de-noising techniques to the results. With an average ratio of 17 between the autocorrelations and the intercorrelations levels, the number of antenna could be increased with a low impact on the image noise level. Several solutions for the miniaturization of the passive device are under study to get highly dispersive and frequency selective channels using metamaterials planar structure and frequency selective surfaces. Using k-space interpolation to decrease the computational time [9], associated to a non-linearly spaced antenna array to increase the imaging resolution [3], this system could be a low-cost solution to achieve real-time high resolution imaging.

References

[1] D.W. Bliss and K.W. Forsythe, "Multiple-input multiple-output (MIMO) radar and imaging: degrees of freedom and resolution." Signals, Systems and Computers, Conference Record of the Thirty-Seventh Asilomar Conference on. Vol. 1. IEEE, 2003.

[2] F.C. Robey, S. Coutts, D. Weikle, J.C. McHarg, and K. Cuomo, "MIMO radar theory and experimental results", IEEE In Sig., Sys. and Comp., Conference on, vol. 1, pp. 300-304, 2004.

[3] J. Li, P. Stoica, K.W. Forsythe, and D.W. Bliss, "MIMO radar signal processing - Part 2 MIMO radar: concepts, performance enhancements, and applications", Wiley, 2008.

[4] M. Klemm, I. J. Craddock, J. Leendertz, A.W. Preece, and R. Benjamin, "Breast cancer detection using symmetrical antenna array", in Proc. EuCAP, pp. 12-16, 2007.

[5] Y. Yang and A.E. Fathy, "Development and implementation of a realtime see-through-wall radar system based on FPGA", IEEE Trans. Geosci. Remote Sens., vol. 47, no. 5, pp. 1270-1280, 2009.

[6] X. Zhuge and A.G. Yarovoy, "A Sparse Aperture MIMO-SAR-Based UWB Imaging System for Concealed Weapon Detection", IEEE Trans. Geosci. Remote Sens. , vol.49, no.1, pp.509-518, 2011.

[7] F. Ramirez-Mireles, "On the capacity of UWB over multipath channels,"IEEE Commun. Lett., vol.9, no.6, pp. 523-525, 2005.

[8] X. Zhuge and A.G. Yarovoy, "Design of low profile antipodal Vivaldi antenna for ultra-wideband near-field imaging" Antennas and Propagation (EuCAP) Proceedings of the Fourth European Conference on. IEEE, pp. 1-5, 2010.

[9] X. Zhuge and A.G. Yarovoy, "Three-Dimensional Near-Field MIMO Array Imaging Using Range Migration Techniques", Image Processing, IEEE Transactions on, vol.21, no.6, pp. 3026-3033, 2012.